Publ. Astron. Soc. Japan **41**, 405–426 (1989)

The Gamma-Ray Burst Detector System on Board Ginga

Toshio MURAKAMI, Masami FUJII, Kiyoshi HAYASHIDA, Masayuki ITOH, Jun NISHIMURA, Takamasa YAMAGAMI, and Atsumasa YOSHIDA

Institute of Space and Astronautical Science, 1-1, Yoshinodai 3-chome, Sagamihara-shi, Kanagawa 229

Jerry P. CONNER, Winifred D. EVANS, Edward E. FENIMORE, Ray W. KLEBESADEL, and Kenneth M. SPENCER

Los Alamos National Laboratory, Los Alamos, NM 87545, U.S.A.

Hiroyuki MURAKAMI

Department of Physics, Faculty of Science, Rikkyo University, Nishi-Ikebukuro, Toshima-ku, Tokyo 171

Nobuyuki KAWAI

The Institute of Physical and Chemical Research, Hirosawa, Wako-shi, Saitama 351-01

Ichiro KONDO

Institute for Cosmic Ray Research, The University of Tokyo, 2-1, Midori 3-chome, Tanashi, Tokyo 188

and

Masahiro KATOH

National Laboratory for High Energy Physics, Oho-cho, Tsukuba, Ibaraki 305

(Received 1988 September 2; accepted 1988 December 23)

Abstract

The system design and in-flight performance of the Gamma-ray Burst Detector (GBD) on board the Japanese X-ray astronomy satellite Ginga (galaxy in Japanese, known as ASTRO-C before the launch) are presented. The satellite was successfully launched on February 5, 1987 from Kagoshima Space Center (KSC) of ISAS. The GBD subsystem started observations on February 26, and it has since then continuously monitored the occurrence of cosmic gamma-ray bursts. It had detected at least 24 gamma-ray burst candidates by the end of March 1988. The number of observed bursts is consistent with the preflight estimation indicating that the instrument is

performing as designed. This paper describes details of the instrument and the in-orbit performance of the detector system, including considerations of background rates and gain stabilities. One example of an observed cosmic gamma-ray burst is also presented.

Key words: Detectors; Gamma-ray bursts.

1. Introduction: Short History and Design Consideration

Since the first report of cosmic gamma-ray bursts in 1973 by the group at the Los Alamos National Laboratory (Klebesadel et al. 1973), 15 years have passed. During this 15-yr interval, many satellite and balloon programs have been carried out and much evidence has been accumulated. The following are the main topics derived from previous observations.

a. Several precise determinations of position for gamma-ray bursts by an interplanetary network (Liang and Petrosian 1986).

b. Discovery of spectral features around several tens of keV and redshifted annihilation lines (Mazets et al. 1981).

c. Possible identification of gamma-ray burst positions with optical flashes which were preserved on archival plates (Schaefer 1981).

In spite of these extensive observations and analyses of the cosmic gamma-ray bursts, the mechanism behind this phenomenon is still unknown, except that there is a widely accepted consensus that a neutron star environment is the origin. A good summary of review papers was compiled during the AIP conference No. 141 held at Stanford University in 1984, and more details of the recent progress of gamma-ray burst studies can be found in the proceedings of that conference (Liang and Petrosian 1986).

Recently, flux increases in the X-ray regime coincident with gamma-ray burst events were detected by spinning satellites monitoring the X-ray sky such as P78-1 (Laros et al. 1984) and Hakucho (Katoh et al. 1984), with the important discovery of a longer-lasting X-ray component. Although the energy region between 30 keV to several MeV has already been observed by several missions, and is being monitored by existing satellites, the X-ray region was not within the range of the instrumentation. There has never before been a gamma-ray burst detector system designed to extend observations to energies less than 30 keV.

Based on the above consideration and the history of gamma-ray burst observations, we decided to direct our effort toward the observation of the X-ray region of gamma-ray burst spectra and the spectral features which are believed to have been observed around several tens of keV. According to this decision, the Gamma-ray Burst Detector (GBD) for the Ginga (or ASTRO-C) satellite was designed to cover the energy range from 1.5 to 500 keV in normal operation mode [for details concerning the satellite and other instruments flown aboard the satellite see Makino and the ASTRO-C team (1987) and Turner et al. (1989)]. Since the weight allotted to the GBD was only 6.5 kg, it was decided to sacrifice the energy region above 500 keV which would have required a much heavier detector with a larger detection area. We tried also to have a wide field of view (difficult for X-ray instruments) in order to observe as many gamma-ray

bursts as possible.

In the following sections, detailed descriptions of the GBD detector system are presented and some results which were obtained in-orbit are described. In section 2, the characteristics of the GBD detectors are described. In section 3, the mechanisms of recording gamma-ray bursts on the satellite and the techniques of data processing are presented. In section 4, the performance of GBD system following launch is compared with that expected prior to launch.

2. Instrument (Sensor)

The satellite Ginga has a mass of about 420 kg. It was placed into an orbit with an apogee of 650 km and a perigee of 550 km (Makino and the ASTRO-C team 1987). The satellite is a 3-axis stabilized type which carries three scientific instruments: the Large Area Counter (LAC), the All Sky Monitor (ASM), and the Gamma-ray Burst Detector (GBD). The Gamma-ray Burst Detector (hereafter referred to as the GBD) of the Ginga satellite consists of four parts. The primary sensors consist of a proportional counter (PC) and a scintillation spectrometer (SC) pointed to a direction parallel to the Z-axis of the satellite, both having wide fields of view. A radiation belt monitor (RBM) and a calibration system (CAL) both using solid state detectors are also included as auxiliary equipment. The block diagram of the GBD system is shown in figure 1. The GBD sensors and their associated analog electronic circuits (FEE) as well as the high voltage supplies (HV's) are integrated as a subsystem which was attached to the top plate of the satellite. The main electronic circuits (ELS), which process all signals from the sensor unit, are contained in another box attached to the center wall of the satellite. The ELS includes logic circuits to detect the occurrence of gamma-ray bursts and also provides information to be stored by high-resolution dedicated memory in the DP (Data Processor) to record the events.

The configuration of the GBD sensor unit is shown in figure 2. The sensors (SC and PC) are mounted, together with the FEE and HV supplies, to a frame (186×331 mm) made of magnesium. This frame is fixed to the top plate of the satellite behind a 150×300-mm aperture which is covered by a thermal insulating sheet of 8.2-μm thick aluminized Kapton to provide a thermal heat shield. The characteristics of the detectors are listed in table 1 and some details are described in the following.

The SC is a scintillation spectrometer using a 1-cm thick NaI (Tl) crystal with an effective area of 60 cm^2. The entrance window of the SC is covered by an aluminum sheet of 0.2-mm thickness. A 7.6-cm diameter phototube (Hamamatsu Photonics R1307) is attached to the crystal via a 3-mm thick glass window and a 15-mm thick light guide made of acrylite. The cylindrical edge of the scintillator cell is covered by a graded shield of copper, silver, tantalum, and the phototube is covered with 0.25-mm Pb in order to reduce the level of background reaching the scintillator from the backside, as shown in figure 3.

The PC is a proportional counter filled with Xenon+CO_2 (10%) at 1.16-atm pressure with a depth of 3 cm and an effective area of 63 cm^2, with an entrance window of 63.5-μm thick beryllium (see figure 4). It is also covered by a graded shield made of tin and molybdenum. It has 4 anode wires of 50-μm gold-plated tungsten wire which are

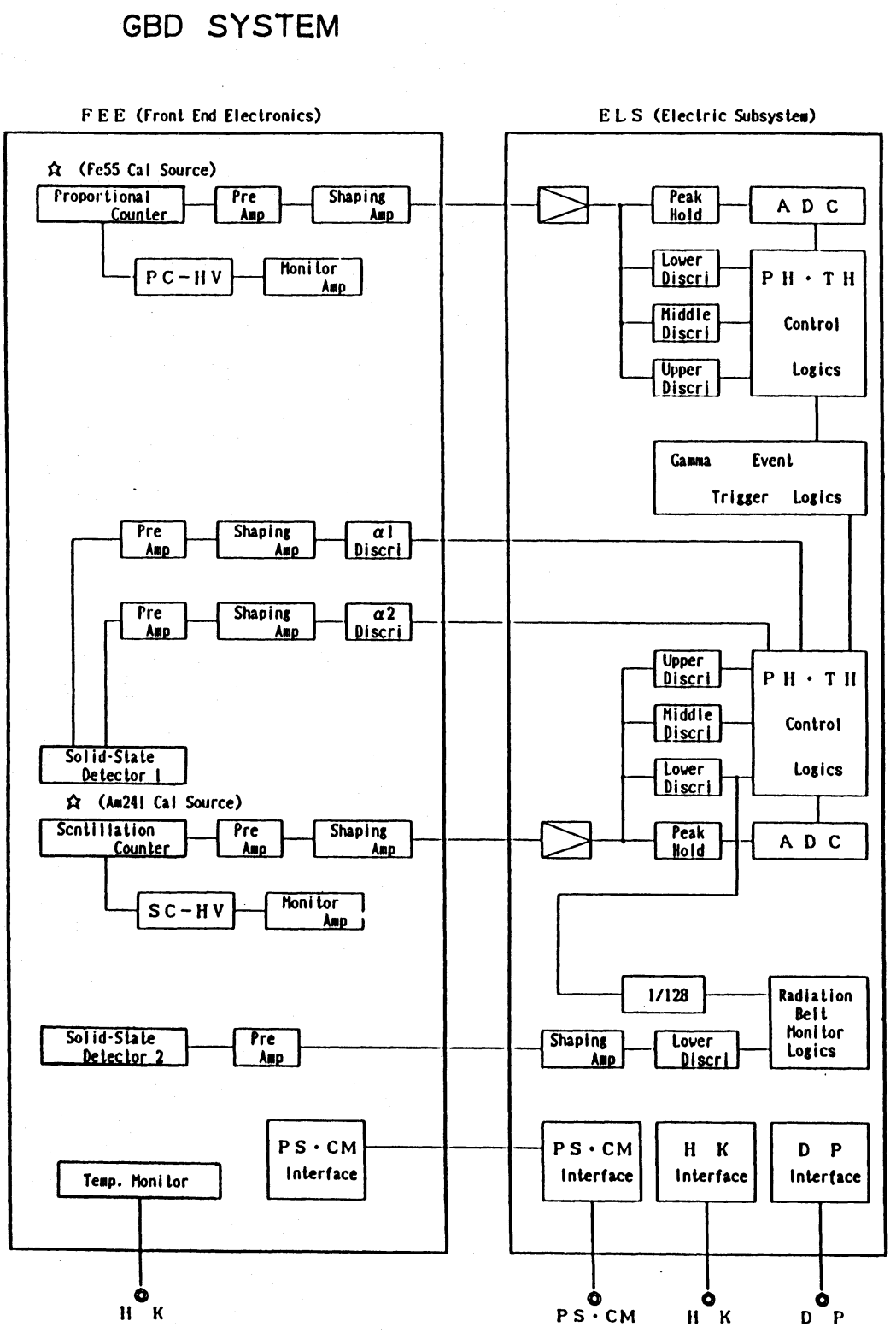

Fig. 1. System block diagram of the GBD. Signal flow and the grouping of the each subsystem are shown. HK indicates housekeeping data. DP represents the central data processor.

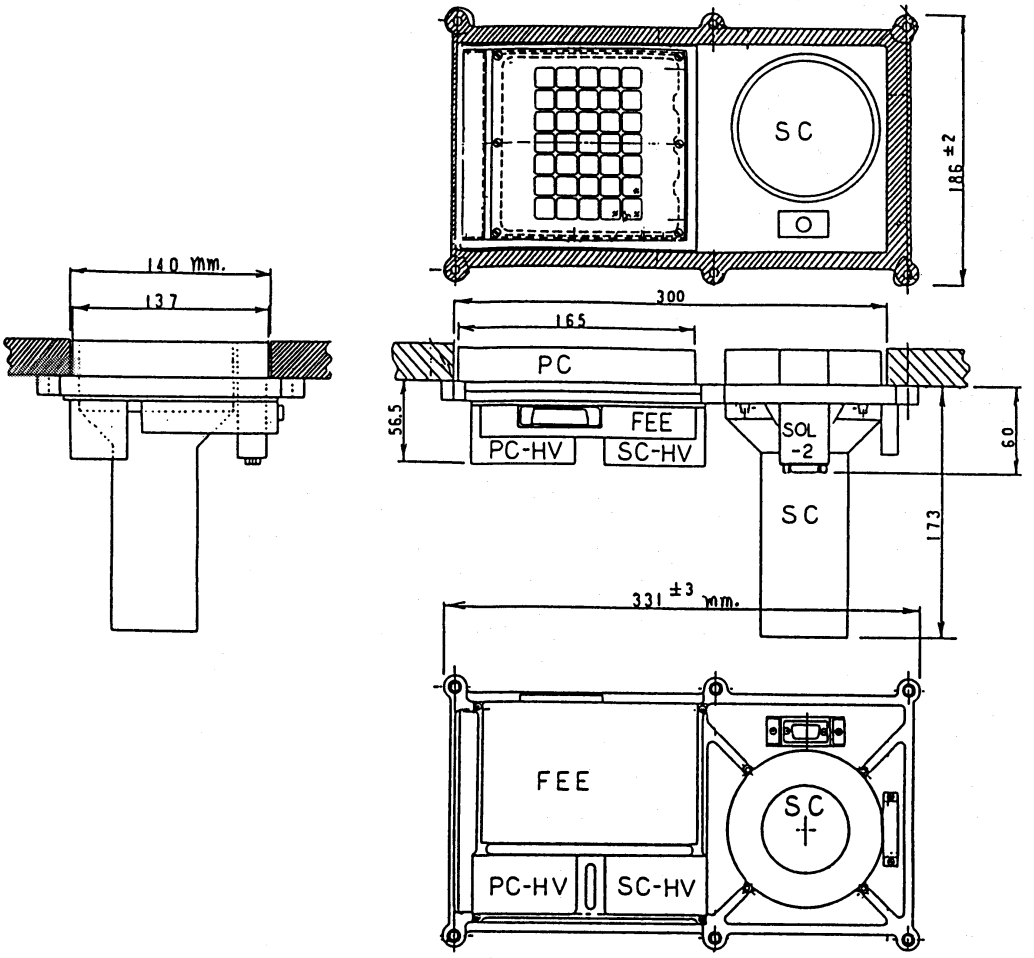

Fig. 2. Three axis projections of the detector system. FEE indicates front-end electronics. All dimensions in this figure are in millimeters.

Table 1. Characteristics of the counters.

Counter name	Material	Thickness	Effective area (cm^2)	Window	Shield
SC	NaI (Tl)	1.0 cm	60	Al (0.2 mm)	Graded shield for the SC (thickness in μm): Cu(254)+Ag(560)+Ta(254)+Pb(690)
PC	$Xe+CO_2(10\%)$	3.0 cm	63	Be (63.5 μm)	Backside shield for the PC (thickness in μm): Sn(127)+Mo(127)

Both counters are uncollimated but have an 8.2-μm thick Kapton thermal shield just in front of the counter. The details of the detector and the shielding materials are shown in figures 3 and 4.

connected together at one end (with a provision for individual gain adjustment), and input to a single amplifier.

In order to cover a large portion of the sky, the PC and the SC have no collimator to limit their fields of view. This design provides the maximum opportunity to detect

Table 2. Time resolution of data (s).

Word bit rate	Real/BDR data			Burst memory
	High	Medium	Low	
SCTH	0.125	1.0	4.0	0.03125
PCTH	0.125	1.0	4.0	0.03125
SCPH	2.0	16.0	64.0	0.5
PCPH	2.0	16.0	64.0	0.5
RBM	0.5	4.0	16.0	···
CAL	32.0	256.0	1024.0	···
SCMON	1.0	8.0	32.0	···
PCMON	1.0	8.0	32.0	···

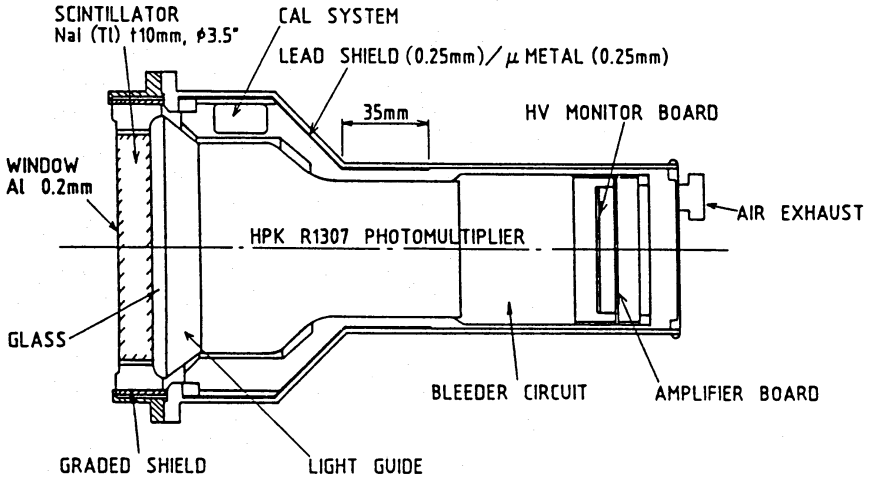

Fig. 3. Details of the SC counter. The NaI (Tl) crystal is covered by a graded shield and the phototube is covered by 0.25-mm thick lead and 0.25-mm mu-metal. The CAL system which emits 60-keV gamma-rays from a radioactive source (^{241}Am) is mounted on the side wall of the sensor housing.

gamma-ray bursts, but at the same time the signal-to-noise ratio in the low-energy region is degraded by contamination from the large flux due to the diffuse cosmic background. This problem was carefully studied by a computer simulation program during the design phase and it was decided to have no collimator beyond the necessary window frame support structure. Shielding materials on the sides and back of the counter body were provided to keep the backside illumination to a minimum.

In normal operation, the energy ranges of the sensors are assigned to be 2–30 keV and 14–400 keV for the PC and the SC respectively, but these can be varied by commands sent from the ground. These energy regions are covered by 16 channels for the PC and 32 channels for the SC, with semilogarithmically spaced bin boundaries. The signals from each detector with a pulse height greater than the lower discriminator level (LD) are analyzed by linear analog-to-digital converters (ADC) with a resolution of 96 and 192 channels for the PC and the SC respectively. The digital output of ADC is then converted to 16 or 32 channels. The linearity of the energy scale in the output

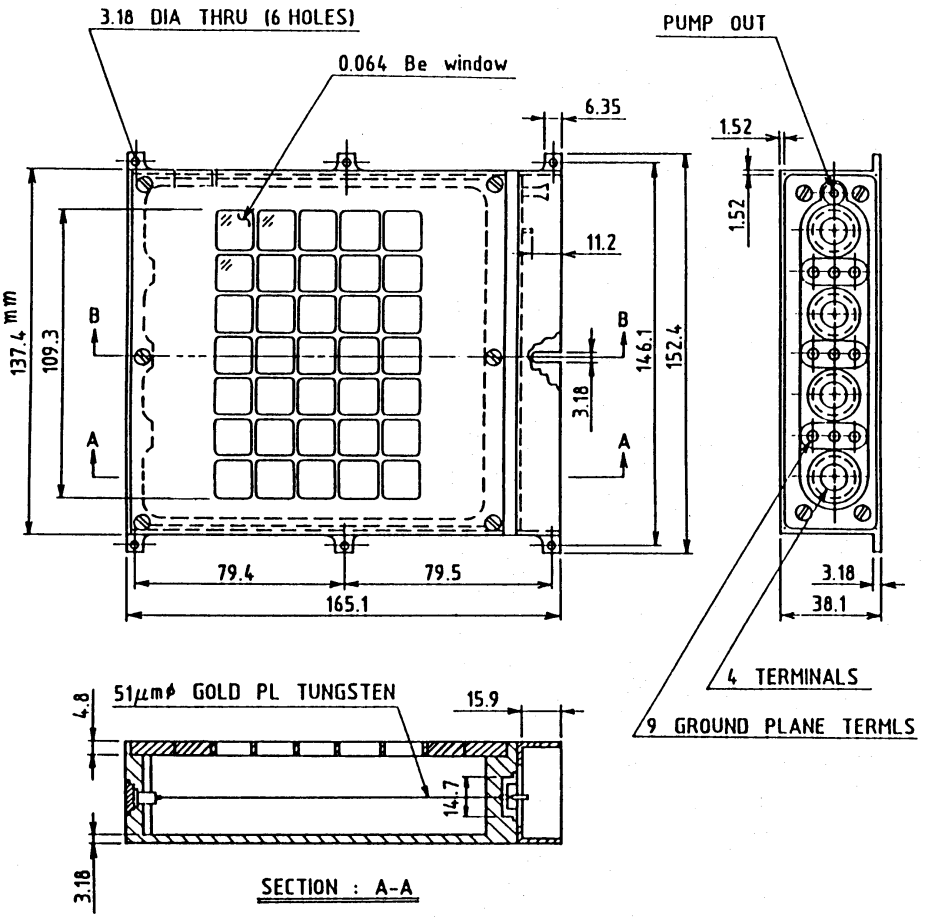

Fig. 4. Details of the PC counter. This counter is entirely covered by a graded shield except for the window. A ^{55}Fe source is mounted on one of the window support ribs for the purpose of calibration. All dimensions are in millimeter.

signal is mainly affected by nonlinearities in the detector response.

In order to observe the spectral features which have been reported to exist around a few tens of keV during gamma-ray bursts, it is important to determine a reliable response function for the system and to use a calibration method which defines the energy scale. The nonlinearity of the SC response (which is commonly observed in scintillation processes) and the escape ratio (which depends highly upon the structure of the counter) were carefully measured and compared with simulated results before the launch. The measured response, exhibiting considerable nonlinearity, and the energy resolution of the SC are shown in figures 5 and 6.

Using this basic information about the response and the structure of the sensors, the effective areas of each as a function of photon energy were estimated by a computer simulation using a Monte Carlo technique. Results of these simulations are shown in figure 7. In figures 7a and b, the effective areas for each pulse height (PH) channel and the integrated effective areas are shown as a function of incident X-ray energy for the PC and the SC respectively. A marked decrease of the effective area of the SC at around 35 keV and of the PC at about 30 keV (caused by the escape of photons at the I and Xe K-shell absorption edges) are clearly seen in the figure. These dips can be

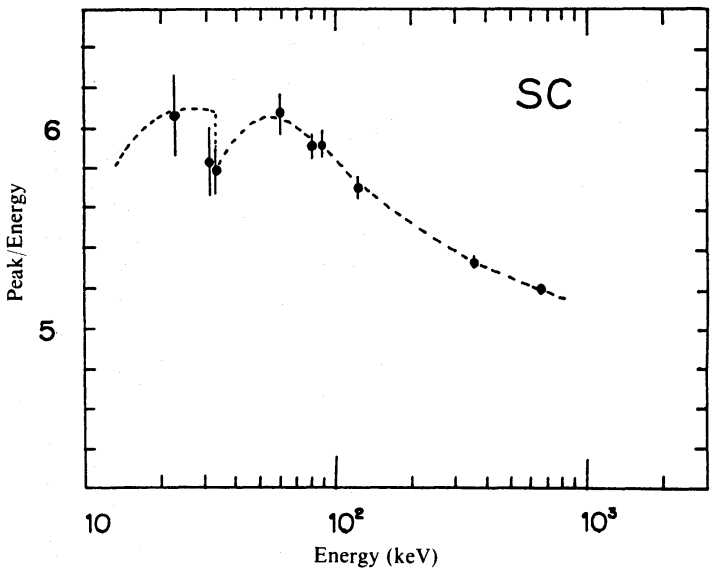

Fig. 5. The SC nonlinearity. The ordinate shows the pulse height of the SC signal divided by the detected energy in arbitrary units as measured in the laboratory.

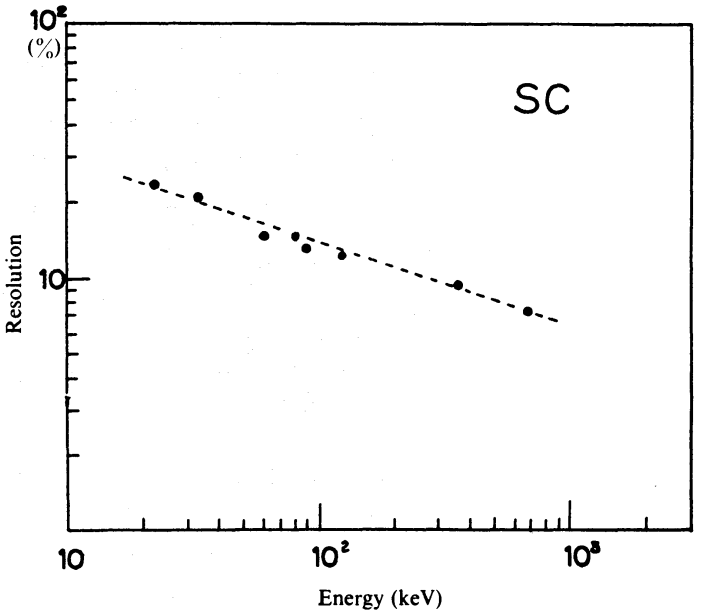

Fig. 6. Energy resolution. The ordinate shows the resolution (FWHM) of the pulse height distribution at the photopeak as measured in the laboratory for gamma-rays of different energies.

confused with real absorption features in the incident gamma-ray spectra when analyzing the data.

The effective areas as a function of incident angles strongly depend on energy. At extremely low and high energy, the effective areas are roughly proportional to the projected area, but at medium energy, the effective areas are the combination of absorption and projected area. In figure 8, the effective areas calculated by a Monte

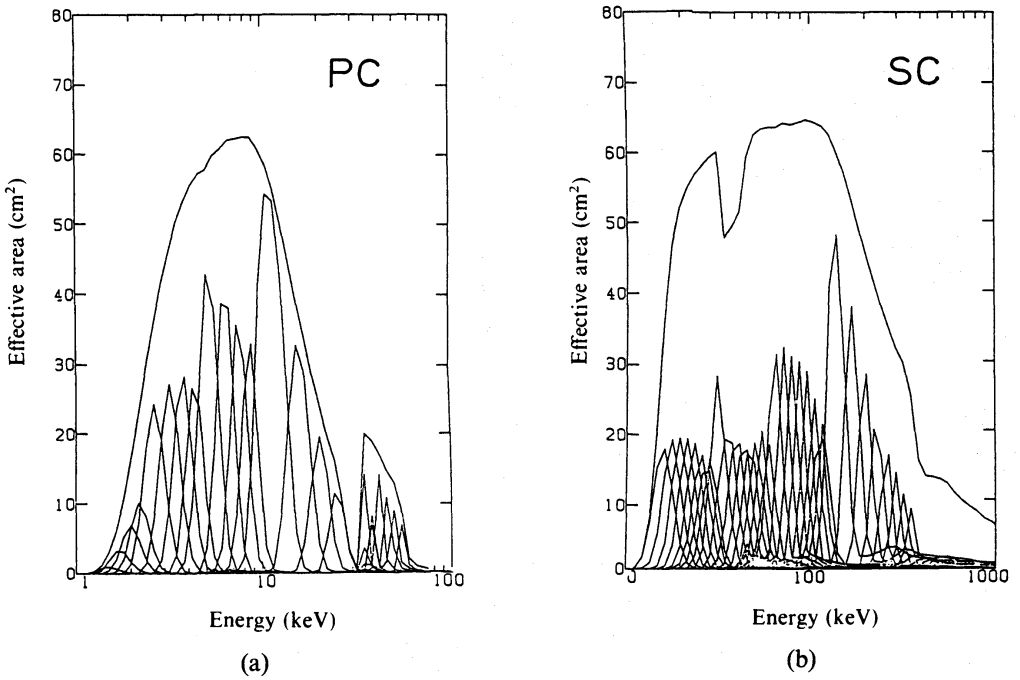

Fig. 7. The effective area for each pulse height channel as computed by a Monte Carlo calculation based on the parameters for structure and materials of the sensors: (a) PC and (b) SC, respectively, as a function of incident photon energy. Envelopes representing the summation of the response from the individual channels defined the total effective area of each sensor. Photons are assumed to be entering the sensors from the direction normal to the entrance window.

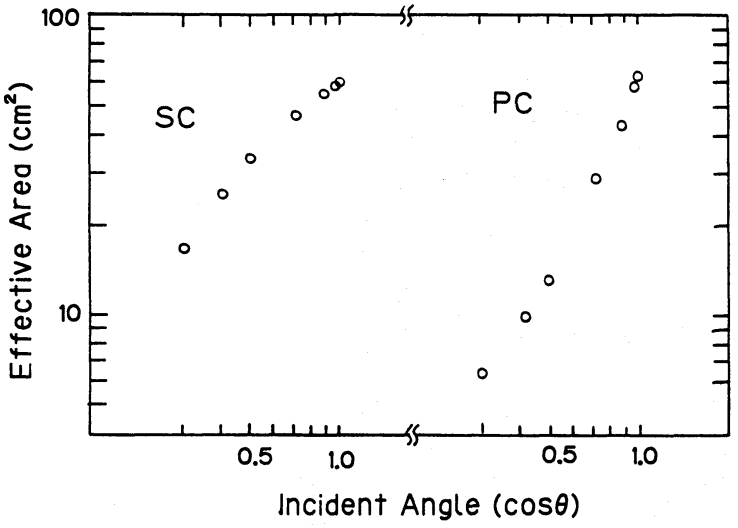

Fig. 8. The effective areas as a function of incident angles for the PC and the SC are calculated by a Monte Carlo method. We require three dimensions for a full display of the effective area for each counter, so only the effective area as a function of incident angles at 100 keV and 8 keV for the SC and the PC respectively are shown .

Carlo method as a function of incident angles of the PC and the SC are shown at 100 keV and 8 keV respectively. The rough field of view of these counters is about 60° (FWHM) at low energy for each counter.

The CAL system (SOL1) is composed of two solid-state detectors with a radioactive ^{241}Am source which emits 60-keV gamma-rays together with alpha particles which can be detected by either one of the solid-state detectors. The output pulses from the solid-state detectors are used for the rejection of CAL-produced gamma-rays from main SC data stream, routing them instead to provide a pulse height spectrum including response to the ^{241}Am gamma-rays separately. For the PC, a weak ^{55}Fe source with a 5.9-keV line with intensity about 1/10 that of the diffuse cosmic X-ray background is attached to the window support structure. The RBM system using another solid-state detector (SOL2) is also included to detect increased fluxes of particles as the satellite passes through the various regions of the radiation belts. This detector has a thickness of 100 microns and 0.9-cm^2 effective area. Any charged particle depositing more than 40-keV energy is detected. Electrons with energies above 90 keV are the main source of counts in this detector, so that it has very high sensitivity for the detection of increases in the charged-particle flux from the radiation belt.

3. Data Processing

Data processing for the GBD is performed on the satellite by two subsystems, namely the GBD-ELS (Electronic subsystem) and the Data Processor (DP). The GBD-ELS receives signals from the SC, PC, RBM, and CAL. These signals are then analyzed to produce time history (TH) as well as pulse height (PH) information. Incoming signals with pulse height between the levels of the lower discriminator (LD) and the upper discriminator (UD) produce pulses to be sent to the DP as TH data. At the same time, the amplitude of each pulse is analyzed by the ADC and converted to 5 or 7-bit pulse-height words to be sent to the DP. PH data for the SC contain one additional bit which indicates coincident arrival of an alpha particle at the CAL detector, thus identifying the response as a calibration pulse.

The gains of the amplifiers as well as the discrimination levels in the ELS can be adjusted by commands sent from the ground through uplink telemetry. Also, the functions of each counter, the HV levels and the data process logic are controlled by the ELS, utilizing commands sent from the ground.

In order to perform the main objective of the GBD system, that is, the detection of cosmic gamma-ray bursts, the ELS has logic circuits to detect the occurrence of a gamma-ray burst while avoiding responses to increases seen in background counting rates due to radiation belt particles.

(a) Burst Detection Logic

In identifying the onset of a gamma-ray burst, a judgment is made by two separate logic circuits which monitor the increase of the counts compared to the background counts ($N_b\,s^{-1}$) taken previously.

In the first circuit, the SC burst flag is generated when counts are accumulated in any one of three trigger intervals dT (0.25, 1, or 4 s) to a level which exceeds the

anticipated accumulation at only background counting rates by more than 8σ or 11.2σ [σ being the standard deviation of the anticipated background counts in the trigger interval, $\sqrt{(N_b dT)}$].

In the second circuit, the PC burst flag is generated when the accumulated counts in a 1- or 4-s interval increase above the background level (taken in the previous 8-s interval) by a fixed amount (predetermined by command to one of 8 possible levels).

The above two logic circuits are enabled or disabled independently. Also, provision is made so that the PC signal can be routed through the SC burst-flag logic or the SC signal to the PC burst-flag logic for crosschecking. The energy region selected to be input to the burst flag logic (between MD and UD) may be controlled by commands so as to optimize the sensitivity to gamma-ray bursts. Also, the threshold counts for the PC flag determination are adjusted by commands to optimize the probability of triggering on gamma-ray bursts. The occurrence of false flags is avoided by inhibiting the burst detection logic if the background counting rate exceeds a level of 768 counts s^{-1} for SC and 3072 counts s^{-1} for PC.

(b) Radiation-Belt Particle Flag Logic

In order to avoid false burst flags due to the effect of radiation belt particles, an RBM flag logic is included in the ELS. This logic monitors the change of counting rate of the RBM detector, and when the counting rate from the RBM exceeds a predetermined count (set to one of 4 levels by command) within an 8-s interval, the RBM flag signal is turned on and stays in that condition until the counts decrease to one half the predetermined flag level. This signal is transmitted to the DP, LAC, ASM, and GBD to indicate to those systems that the satellite is operating within a radiation belt. This flag is made available so that the high voltage supplied to the proportional counters can be reduced to avoid damage from excessive counting rates, and also to inhibit the burst flag logic, avoiding false events.

(c) System Control

In order to control the operating parameters of the GBD system, command signals are provided from the spacecraft to the ELS. Two kinds of command signals, Discrete Commands (DC) and Block Commands (BC), are used depending on the importance and complexity of the desired actions.

DC's are used to activate one action per execution of one command, so are usually used to activate one action such as "on/off" or "enable/disable." Eleven DC's are used for the GBD mainly to switch on/off several parts of the system. DC's can also be stored in a program command memory so that they can be activated at any part of the orbit regardless of visibility from KSC where these command are relayed to the satellite through up-link telemetry.

BC's are composed of 8-bit signal codes preceded by 8-bit address codes to specify a particular operation. GBD uses 6 BC's to control operating functions of the GBD system such as the gains of the amplifiers, discriminator levels, burst detection thresholds etc.

(d) Data Processing by the DP

Using the signals and flags generated by ELS, the on board data processor system

(DP) handles the final data processing for the GBD. In normal mode, the DP collects data from all subsystems on the satellite and formats them into the data stream to be sent to real-time telemetry (TLM) as well as to the bubble-memory data recorder (BDR) for subsequent telemetry to KSC. The bit rates for the real-time telemetry and for the storage of data into the BDR are the same and are controlled by commands stored in the programmed memory according to an observation plan for the X-ray detectors (LAC and ASM), which is drawn to use the limited capacity of the BDR (40 Mbits) most effectively. In normal mode, GBD data are edited into the real-time data at a rate of 4 words/frame (8 bits/word, 64 total words/frame) at a rate of 16, 2, or 0.5 kbps, depending on the operating mode. The data are also stored in the BDR, if it is in record mode. In order to record gamma-ray burst data with high detection efficiency regardless of the operating mode, the DP also has capability to store data for triggered events in a RAM memory, with high time resolution.

(e) Gamma-Ray Burst Data in RAM Memory

Since the occurrence of a gamma-ray burst is unpredictable, it is necessary to monitor GBD data almost continuously, and record the background data in the RAM memory in a cyclic mode until the occurrence of a gamma-ray burst is detected. When the occurrence of a gamma-ray burst is sensed by the flag logic, data recorded during the previous 16(32) s, together with data acquired during the 48(96) s following the onset of the gamma burst flag, are retained in the RAM memory. Time History (TH) data with time resolution of 31.25 ms and Pulse Height (PH) data with time resolution of 0.5 s are recorded in the memory. When the counting rate of the SC signal exceeds a limit (variable upon command, but normally 2,048 counts s^{-1}), the time interval for accumulation of the set level (normally 64) of counts is recorded in the TH data word instead of the count accumulation itself. This "time-to-spill" mode of data acquisition is adopted to improve the temporal resolution of the measurements during the maximum intensity of very large gamma-ray bursts. The onset time of the burst flag, relative to the spacecraft clock, is also recorded in the RAM memory to an accuracy of 244 μs. The stored data are metered out to the telemetry data stream while the spacecraft is over the receiving station (KSC), a process initiated by the "memory playback" command (normally done 5 times per day).

(f) Real-Time Data

In order to assess the background counting rates and energy spectra, it is necessary to monitor these functions during normal operation. For this purpose, 4 words/frame (duration of 0.0625, 1, or 8 s per frame, depending upon the data rate selection) are assigned to the GBD real-time data. Counting rates (TH) of the SC and the PC are monitored with one word, giving time resolution of two frames, and 2 words are used to transmit pulse height distributions taken during 32 frame time intervals. Also, counting rates within the trigger flag energy range and counts above UD level as well as those of CAL and RBM detectors are monitored with time resolution of 4 to 16 frames.

In the low bit-rate mode, the accumulated counts may exceed the capacity of a data word, so it is necessary to prescale the TH count and to provide a bit compression

scheme for pulse height data. For TH data from both the SC and the PC, as well as for PH data from the SC, a compression scheme codes the contents of 12 bit scalers into 8 bits in order to use the allocated telemetry more effectively.

In order to monitor the operating conditions of the GBD system, several housekeeping data such as the temperature of the detectors and the output voltage of HV supplies are telemetered at longer intervals.

4. In-Orbit Performance

(a) Background Level

The HV power supplies of the GBD were switched-on on February 26, 1987 following a long period to allow outgassing from the satellite and after a check of the function of RBM which protects the gas counters on board from high charged-particle background (high background causes more rapid degradation of the gas). The background counting rates, which are mainly due to the diffuse cosmic background, have been found to be similar to the rates which were estimated before launch. Typical values of the background counting rates are about 1100 counts s^{-1} for the PC (1.5 to 28 keV) and 560 counts s^{-1} for the SC (14 to 375 keV) at times when the field of view is free from earth occultation and outside high particle background regions such as SAA (South Atlantic Anomaly). Based on these background rates and a classical gamma-ray burst spectrum, the minimum detectable gamma-ray burst size is estimated to be about 5×10^{-7} erg cm^{-2} for a burst of 1-s duration for the SC which has the better signal to noise ratio.

(b) Pulse Height vs. Energy Relationship

The CAL peaks in the PC and SC pulse height spectra, shown in figure 9, are obtained when these counters look toward the earth's surface, for then background counting rates are minimized. The positions of these peaks show no significant change compared with data taken before launch. The CAL response has been continuously monitored since the launch, and no change in gain greater than 1% had been detected up to the end of October, 1987, as shown in figure 10. Thus, we assigned the energy calibrations using data taken before launch. The reliability of this energy assignment for each channel has been checked using the pulse height spectra of activation lines which are observed during the passage of the SAA as shown in figure 11. Many activation lines such as iodine (30, 68, 191 keV), tin (53, 187 keV) and tellurium (145 keV) are identified (Dyer et al. 1980). The positions of these lines are consistent with previous results such as those obtained by HEAO-A (Knight 1981). The energy assignments in figure 11 include the nonlinearity of the SC counter measured before the launch. Using this established energy scale, we have checked the spectrum observed for the Crab Nebula and obtained the best fit parameters for a single power-law function as $(1.0 \pm 0.1)E^{-1.9 \pm 0.1}$ photons $s^{-1}\,cm^{-2}\,keV^{-1}$. This spectrum, shown in figure 12, is consistent with the results from the LAC (Turner et al. 1989) and those from previous satellites. It is clear from this result that there is no spectral structure caused by an instrumental effect for the Crab spectrum around several tens of keV. However, GRB's exhibit much harder spectra, and more analysis is needed to confirm that no

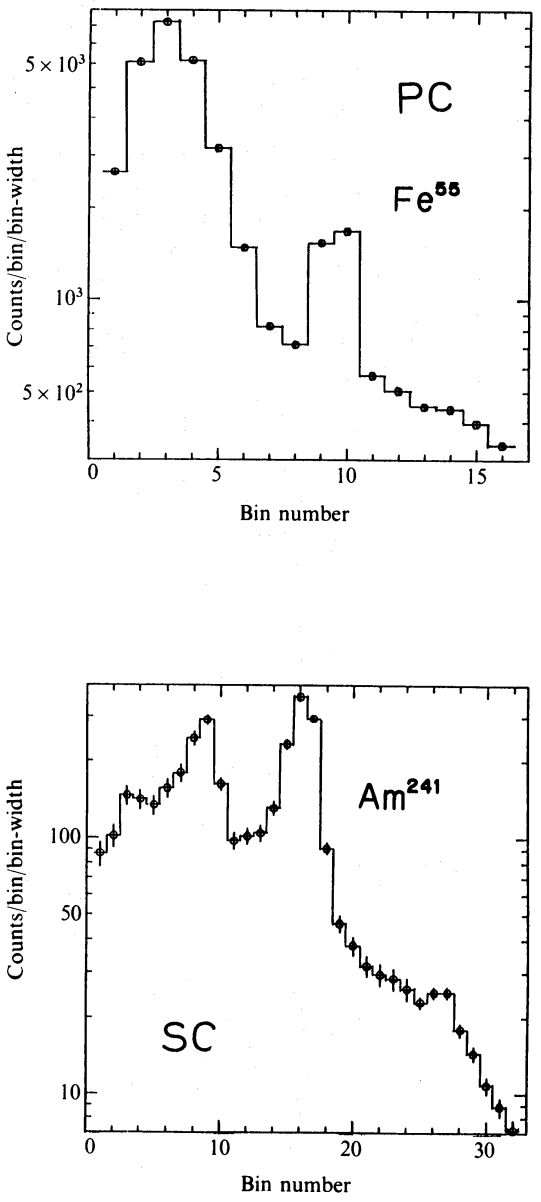

Fig. 9. Pulse height distributions in the PC and the SC recorded when the sensors were looking toward the earth (diffuse X-ray background is negligible). For the SC, only pulses coincident with an output pulse from the CAL detector are used to get this pulse height distribution. Peaks from induced radioactivity, which can also be used as the energy references, are clearly seen in the figure.

instrumental effects exist which might distort those spectra.

(c) Gamma-Ray Burst Detection and False-Event Rejection.

The threshold levels of the SC gamma-ray burst flag are conservatively selected at 11.2σ. Many false events are generated and occupy the burst memory when the 8.0σ level is used as the threshold because of the background fluctuations and because of charged particle events such as precipitating electrons and electrons trapped in the

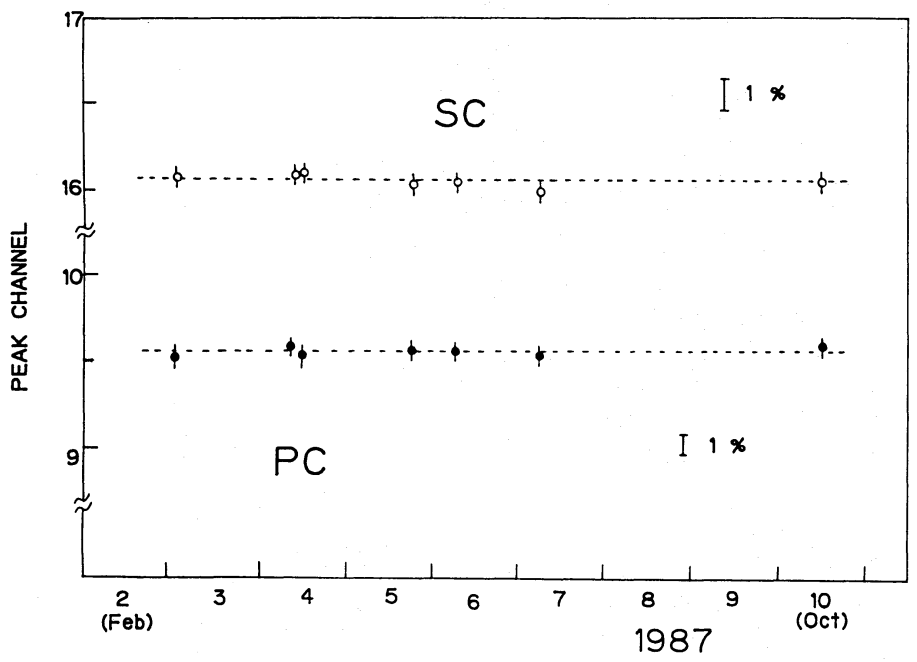

Fig. 10. Stability of gain (or CAL peak) after the launch. Since the launch on February 5, 1987, the gain of each counter has been continuously monitored using the CAL peak produced by the radioisotopes as plotted in this figure. There is no sign of any gain change greater than 1%.

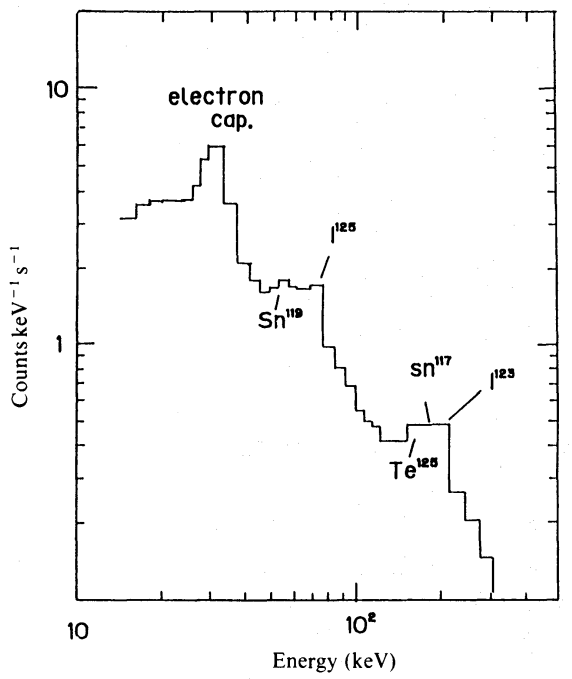

Fig. 11. Activation lines in the SC data. When the satellite passes through the SAA, NaI and other material surrounding the scintillator are activated. Decay gamma-rays from these activated materials are then detected in the SC PH data. There are lines identified as gamma-rays from ^{119}Sn, ^{125}I, ^{125}Te, ^{117}Sn, and ^{123}I.

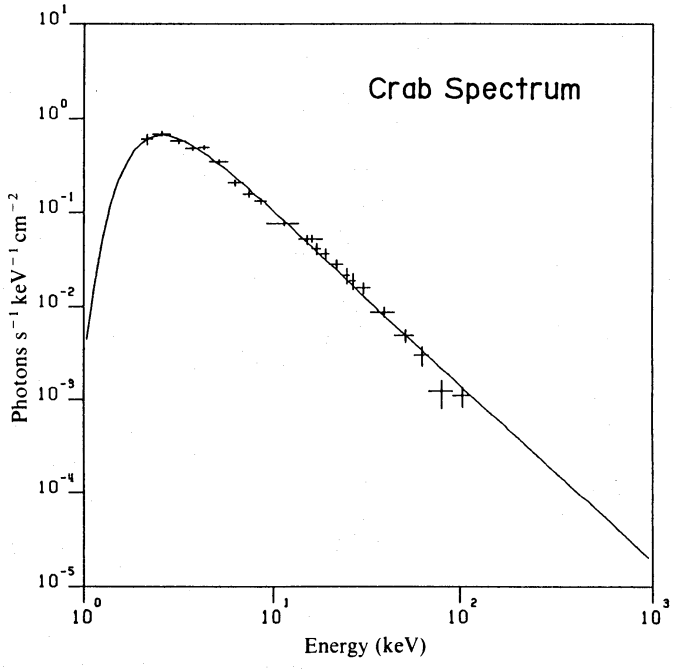

Fig. 12. A calibration from observed data of the Crab Nebula, using the established energy scales and effective areas. The derived best fit parameters for the resulting spectrum are $(1.0\pm0.1)E^{-1.9\pm0.1}$ photons s^{-1} cm^{-2} keV^{-1}. This is consistent with results from the LAC and from previous satellites. It is clear from this result that there is no spectral structure produced by instrumental effects.

plasma bubbles. The PC flag logic is not enabled at present because of frequent false events not only caused by the charged particle events but also caused by cosmic X-ray sources emerging from the shadow of the earth. This latter mechanism gives rise to a sudden increase of counts in the soft X-ray region, and produces a false burst event in the PC burst logic.

The orbit of Ginga is inclined at 31°, thus, during 5 to 6 of the 15 orbits a day, it passes the SAA region. During these passages, the gamma-burst flag logic is inhibited by the RBM system to avoid false event flags caused by high particle background as shown in figure 13. This logic has been found to be working sufficiently well. One prominent and frequent feature observed in background counting rates, which produces a false event, was found to be associated with the presence of plasma bubbles in the lower magnetosphere. We call the distinctive signature observed in the increase of counting rates due to particles trapped in plasma bubbles the "horn of the bull" because of its similarity in shape. Since the characteristics of these responses are very similar in time scale to that of some of real gamma-ray bursts, it is very difficult to avoid recording false events, even by adjusting parameters for the GBD flag logic.

(d) Observation by the Ginga Satellite

Since Ginga was put into operation on February 26, 1987, it has performed observations of many X-ray sources using the LAC and the ASM almost continuously. The attitude of the satellite is controlled to point the LAC (Y-axis) to a particular

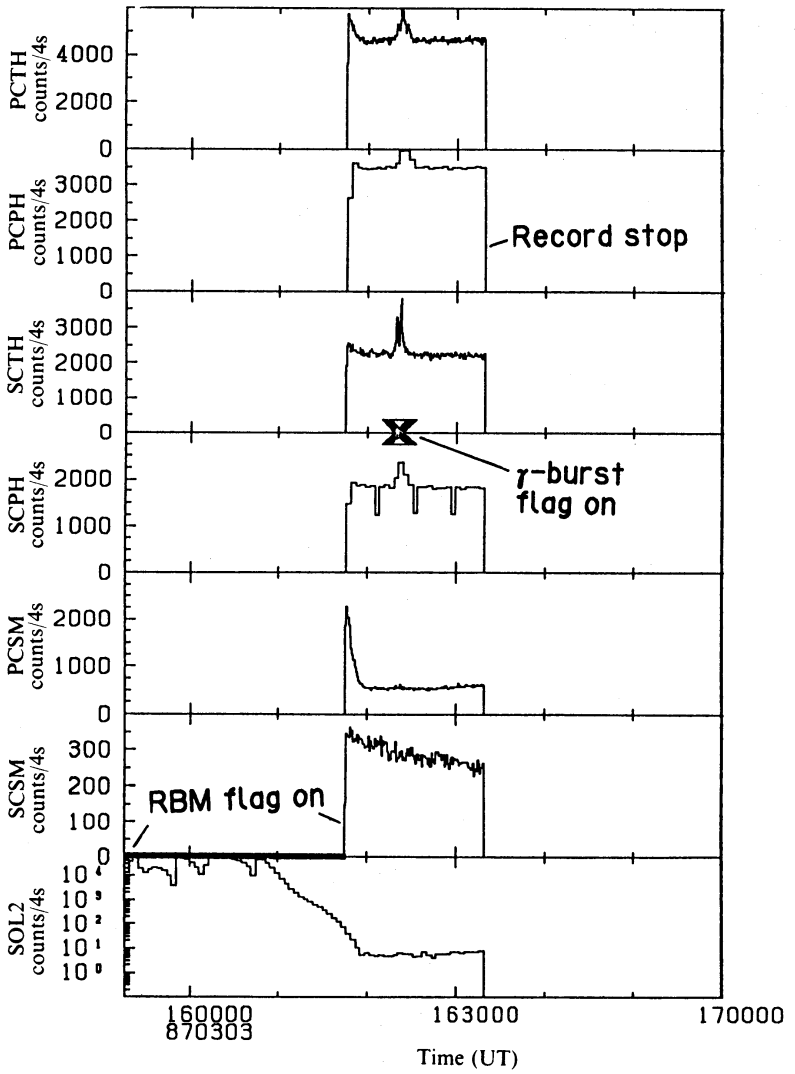

Fig. 13. An example of data stored in the bubble-memory data recorder (BDR). This is the first recorded gamma-ray burst on March 3, 1987. Typical background rates are also shown in the figure before and after the gamma-ray burst. The "X" mark indicates the time when the burst flag was set. A black bar in the last curve indicates that the RBM flag is set due to high charged-particle counts. Part of the RBM data shows an overflow of counts over the maximum capacity of the scaler (65,535 counts/4 s).

source to be observed during each observation period. The occurrence of SN 1987A in the LMC allowed an opportunity to monitor the X-ray flux from a nearby supernova using the LAC in scan and point mode. A constraint for the orientation of the Z-axis is imposed by the limitation that the angle between the solar direction and Z-axis should be less than 45°. These conditions have restricted the direction of the center of the field of view (FOV) of the GBD detector [see for more detail, Makino and the ASTRO-C team (1987)]. Telemetry contacts with the satellite are made from KSC five times per day lasting up to 14 min/pass. During these passes, the data stored in the gamma-ray burst memory, together with background data stored in the BDR, are sent to the ground station. The received data are checked both at KSC and ISAS using a quick-look display

and burst-search software. Although there are typically a few events per day typically recorded in the burst memory, most are found to be false events. After careful comparison of data from the SC and the PC with those of SOL2, many events were rejected as being caused by an increase in the charged particle flux or by fluctuations in the background X-ray flux.

(e) Observed Gamma-Ray Burst Candidates

The GBD has detected at least 24 events which remain as gamma-ray burst candidates after carefully inspecting the observed data. For some of the events, confirmation was obtained by observations made by other spacecraft such as SMM (E. Rieger, private communitcation) and PVO (R. Klebesadel, private communication). A complete list of gamma-ray burst candidates will appear in a separate paper (Yoshida et al. 1989). The event shown in figure 13 was observed on March 3, 1987, using data stored in the BDR together with those in the RAM memory. The curves shown in this figure are taken from records stored in the BDR, and demonstrate the sequence of events which occurred before and after the event. The bottom curve in this figure shows the variation of the counting rate of SOL2 (RBM). At the beginning of the graph these data indicate that the satellite was in a high particle background region, consequently the HV supplies to the PC and the SC were shut down and no counts are shown in the lower curves. At about 16:18 UT, the RBM counting rate became sufficiently low to allow HV supplies to return to normal levels. The SC gamma-ray burst flag was then set at 16:23 UT as shown by the "X" (PC burst logic was disabled). The data in the BDR were terminated at about 16:35 when the satellite was commanded from KSC to telemeter the recorded data.

The contents of GBD RAM memory recorded during this event are shown in figure 14. These data span the time interval from -16 to $+48$ s relative to the burst onset time for SC TH data, and the interval from -32 to $+96$ s for PC TH data. The time resolution available from the RAM data is 31.25 ms for TH and 0.5 s for PH data respectively. In this plot TH data are shown with 0.5-s (a, b) and 62.5-ms (c, d) time resolution. Intensity variations with time durations down to 62.5 ms are evident, although they are masked by large statistical fluctuations. It is also noted that the burst consisted of several peaks with time durations of several seconds which are especially pronounced in the SC. The fact that the intensity increase of the signal in the PC becomes more pronounced at later times in the burst suggests spectral softening with time. The observed pulse height spectrum based on a limited portion of the burst is shown in figure 15. The open circles indicate the PC and the small squares indicate the SC data. It is clear from this figure that the observed response of the two sensors intersects at around 16 keV as expected from the calculation of efficiencies as a function of photon energy. This indicates that the detectors are performing properly. It is also noted from this figure that there are clear spectral features at around 20 keV and 40 keV. Using the detector response, incident photon fluxes were deconvolved from the observed counting rates. The observed photon distribution of the incident flux shows a good fit to a thermal cyclotron-type spectrum with two absorption lines as seen in figure 16. This is interpreted as a cyclotron harmonic structure in a strong magnetic field of an order of 10^{12} G [for more details, see Murakami et al. (1988) and Fenimore et al.

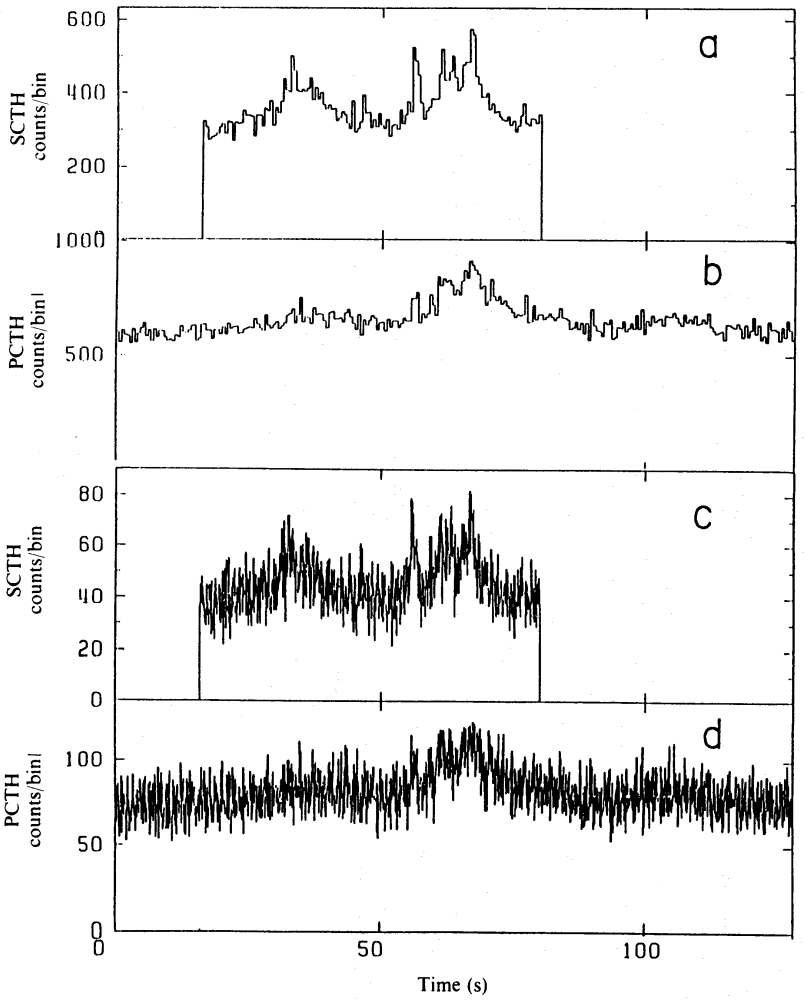

Fig. 14. An example of data stored in the burst RAM memory. The data as recorded in the burst RAM memory for the event shown in figure 13. The original data were taken with 31.25-ms time resolution, but in this figure, counts have been summed over 0.5 s (for a and b) and 62.5 ms (for c and d) are shown. Data for the time interval from −16(−32) s to 48(96) s relative to the onset of burst are stored into burst memory for SC(PC), respectively.

(1988)]

5. Summary

A gamma-ray burst detector system (GBD) on board the astronomical satellite Ginga was designed and built to observe cosmic gamma-ray bursts over a wide range of energy (1.5 to 400 keV) with high detection sensitivity.

The characteristics of the detector system, signal and data processing on board the satellite have been described.

After the satellite was placed into near eath orbit (31° inclination, 650-km apogee, and 550-km perigee), the GBD system was carefully tuned and has been working satisfactorily since. Examination of returned data shows that the characteristics of the GBD system have remained stable since launch. The gamma-ray burst detection logic

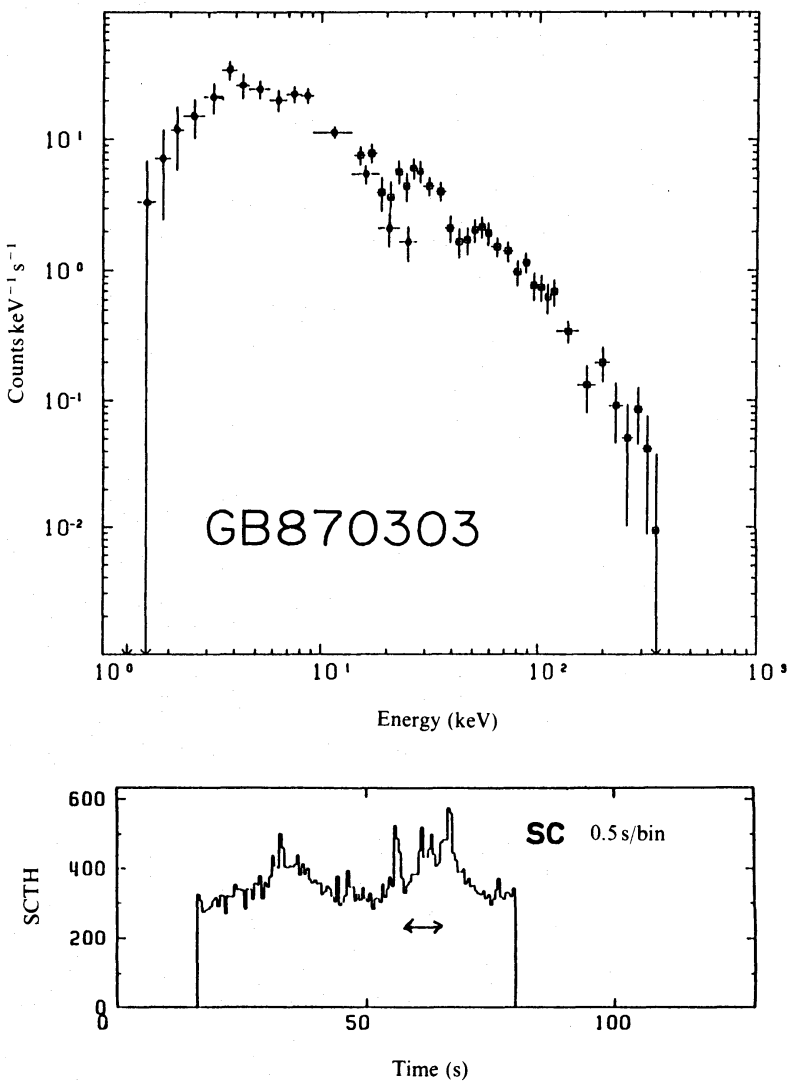

Fig. 15. Observed pulse height spectrum at the limited portion of the March 3, 1987 event. The net contribution above the background level for the PC and the SC are plotted as functions of the energy deposited in the sensors. PC and SC spectra intersect each other at around 16 keV as expected from the numerical calculation of the effective area. At least 8 channels of the SC and 3 channels of the PC counter are overlapped. It is noted that there are two spectral structures at around 20 keV and 40 keV which were not seen in the Crab Nebula spectrum.

(with parameters carefully selected) has proved to have a high detection probability for gamma-ray bursts, while adequately rejecting false events due to increases in the flux of charged particles.

So far, about 24 candidate gamma-ray burst events have been identified during one year of observation. Two events among them showed a possible cyclotron absorption feature with harmonics at about 20 and 40 keV in energy (Murakami et al. 1988; Fenimore et al. 1988). The rate of detection is consistent with the result of computer simulations at a threshold of 5×10^{-7} erg cm^{-2}.

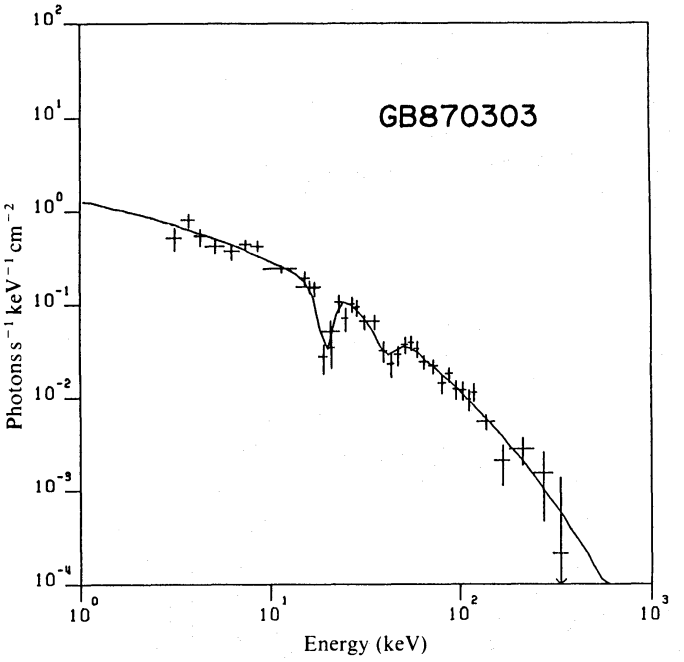

Fig. 16. Deconvolved incident spectrum of figure 15. This analysis uses the response functions derived through the numerical calculations and the Crab Nebula calibration. The energy response of PC is assumed to be a gaussian shape and that for SC was derived by the Monte Carlo simulation. It is clear that two absorption lines at 20 keV and 40 keV are required to have a good fit for this event. [For more details of this structure, see Murakami et al. (1988) and Fenimore et al. (1988).]

The authors gratefully acknowledge Professors M. Oda, F. Makino, and Y. Tanaka for arranging this GBD system as an international collaboration between the Institute of Space and Astronautical Science and the Los Alamos National Laboratory, and also for supporting the successful implementation of this instrument. The GBD was developed through the resourceful effeorts of many engineers and technicians. We especially wish to thank Mrs. M. Piotrosky and G. Obbink at Los Alamos and H. Temple at the Sandia National Laboratories-Albuquerque. Additionally, we wish to thank the staff and the engineers of ISAS who were responsible for developing and launching the Ginga satellite. Finally, the authors thank the Ginga operation team who are efficiently conducting the operation of the Ginga satellite day and night. The data presented in this paper have been provided through the efforts of this team.

References

Dyer, C. S., Trombka, J. I., Seltzer, S. M., and Evans, L. G. 1980, *Nucl. Instrum. Methods*, **173**, 585.

Fenimore, E. E., Conner, J. P., Epstein, R. I., Klebesadel, R. W. Laros, J. G., Yoshida, A., Fujii, M., Hayashida, K., Itoh, M., Murakami, T., Nishimura, J., Yamagami, T., Kondo, I., and Kawai, N. 1988, *Astrophys. J., Letters*, **335**, L71.

Katoh, M., Murakami, T., Nishimura, J., Yamagami, T., Fujii, M., and Itoh, M. 1984, in *High Energy Transients in Astrophysics*, ed. S. E. Woosley (American Institute of Physics, New York), *AIP Conference Proc. No. 115*, 390.

Klebesadel, R. W., Strong, I. B., and Olson, R. A. 1973, *Astrophys. J. Letters*, **182**, L85.
Knight, F. K., 1981, Ph. D. Thesis, University of California, San Diego.
Laros, J. G., Evans, W. D., Fenimore, E. E., Klebesadel, R. W., Shulman, S., and Fritz, G. 1984, *Astrophys. J.*, **286**, 681.
Liang, E. P., and Petrosian, V. 1986 (ed.), *Gamma-Ray Bursts, AIP Conference Proc. No. 141* (American Institute of Physics, New York).
Makino, F., and the ASTRO-C team 1987, *Astrophys. Letters Commun.*, **25**, 223.
Mazets, E. P., Golenetskii, S. V., Aptekar', R. L., Gur'yan, Yu. A., and Il'inskii, V. N. 1981, *Nature*, **290**, 378.
Murakami, T., Fujii, M., Hayashida, K., Itoh, M., Nishimura, J., Yamagami, T., Conner, J. P., Evans, W. D., Fenimore, E. E., Klebesadel, R. W., Yoshida, A., Kondo, I., and Kawai, N. 1988, *Nature*, **335**, 234.
Schaefer, B. E. 1981, *Nature*, **294**, 722.
Turner, M. J. L., Thomas, H. D., Patchett, B. E., Reading, D. H., Makishima, K., Ohashi, T., Dotani, T., Hayashida, K., Inoue, H., Kondo, H., Koyama, K., Mitsuda, K., Ogawara, Y., Takano, S., Awaki, H., Tawara, Y., and Nakamura, N. 1989, *Publ. Astron. Soc. Japan*, **41**, 345.
Yoshida, A., Murakami, T., Itoh, M., Nishimura, J., Tsuchiya, T., Fenimore, E. E., Klebesadel, R. W., Evans, W. D., Kondo, I., and Kawai, N. 1989, *Publ. Astron. Soc. Japan*, **41**, 509